

RESEARCH ARTICLE

10.1002/2015WR017199

Key Points:

- Richards' and overland flow approaches similarly simulate subsurface stormflow
- Infiltration excess subsurface stormflow (SSF) can occur along the bedrock surface
- SSF and overland flow show similar behaviors in terms of the role of their lower boundaries

Correspondence to:

A. A. Ameli,
aaameli@uwaterloo.ca

Citation:

Ameli, A. A., J. R. Craig, and J. J. McDonnell (2015), Are all runoff processes the same? Numerical experiments comparing a Darcy-Richards solver to an overland flow-based approach for subsurface storm runoff simulation, *Water Resour. Res.*, 51, doi:10.1002/2015WR017199.

Received 6 MAR 2015

Accepted 15 NOV 2015

Accepted article online 18 NOV 2015

Are all runoff processes the same? Numerical experiments comparing a Darcy-Richards solver to an overland flow-based approach for subsurface storm runoff simulation

A. A. Ameli^{1,2}, J. R. Craig¹, and J. J. McDonnell^{2,3}

¹Department of Civil and Environmental Engineering, University of Waterloo, Waterloo, Ontario, Canada, ²Global Institute for Water Security, School of Environment and Sustainability, University of Saskatchewan, Saskatoon, Saskatchewan, Canada, ³School of Geosciences, University of Aberdeen, Aberdeen, UK

Abstract Hillslope runoff theory is based largely on the differentiation between infiltration excess overland flow, saturation excess overland flow, and subsurface stormflow. Here we explore to what extent a 2-D friction-based overland flow model is useful for predicting hillslope-scale subsurface stormflow, posited here as phenomenologically the same as infiltration excess at depth. We compare our results to a 3-D variably saturated Darcy-Richards subsurface solver for individual rainfall runoff events. We use field data from the well-studied Panola Mountain Experimental hillslope in Georgia USA. Our results show that the two models are largely indistinguishable in terms of their ability to simulate the hillslope hydrograph magnitude and timing for a range of slopes and rainfall depths. Furthermore, we find that the descriptive ability of the overland flow model is comparable to the variably saturated subsurface flow model in terms of its ability to represent the spatial distribution of subsurface stormflow and infiltration across the soil-bedrock interface. More importantly, these results imply that the physics of infiltration excess subsurface stormflow at the soil-bedrock interface is similar to infiltration excess overland flow at the soil surface, in terms of detention storage, loss along the lower boundary, and threshold-like activation at the larger hillslope scale. Given the phenomenological similarity of overland flow and subsurface stormflow and the fact that overland flow model predictions are considerably faster to run (particularly as slope and rainfall depth increase), these findings imply that new forms of hillslope-scale subsurface storm runoff predictions may be possible with the knowledge of bedrock permeability and limited soil information. Finally, this work suggests that the role of soil mantle vis-à-vis subsurface stormflow is mainly as a filter that delays the development of patches of saturation along the bedrock surface. Our model results show that simple realizations of soil based on a few soil depth measurements can possibly be enough to characterize this filtering effect.

1. Introduction

Many factors control the disposition of storm rainfall and snowmelt. Assessing the hierarchy of these factors and their relative importance in different environments is exceedingly difficult with today's theory and measurement technology [Jencso and McGlynn, 2011]. We know that natural hillslopes are complex systems with threshold-like behavior, hysteresis, feedbacks, and other characteristic forms of nonlinearity [Beven, 2006; McDonnell et al., 2007]. It is common therefore to consider all hillslope runoff forms as threshold processes. For overland flow, the threshold response to precipitation occurs after the emergence of patches of saturation on poorly permeable soil [e.g., Antoine et al., 2009; Fiedler and Ramirez, 2000] or on areas saturated from below from a rising (permanent or perched) water table [e.g., Frei and Fleckenstein, 2014; Frei et al., 2010; Loague et al., 2010; Mirus and Loague, 2013]. As the precipitation event progresses, the ponded areas expand, connect to other downslope ponded patches until there is hillslope-scale "connectivity" and lateral overland flow at the slope base is produced [Chu et al., 2013]. Such overland flow (infiltration excess or saturation excess) is largely controlled by soil surface (micro, meso, and macro) topography and soil permeability.

Subsurface stormflow response to precipitation is also a threshold-like process [e.g., Peters et al., 2003; Tromp-van Meerveld and McDonnell, 2006b] that depends upon the microtopography, mesotopography, and macrotopography—not of the surface topography but the topography of the restricting layer at depth

(e.g., soil-bedrock interface, soil-argillic interface, etc.). Phenomenological descriptions of subsurface stormflow summarize it as a process initiated by filling and spilling of the small-scale depressions at the soil-bedrock interface [e.g., *Spence and Woo*, 2003; *Tromp-van Meerveld and McDonnell*, 2006b], followed by growth and ultimately, hillslope-scale connectivity of patches of transient saturation. This connects the upslope areas with the base of the hillslope through organized subsurface topographically controlled networks along the soil-bedrock interface.

McDonnell [2013] has argued that infiltration excess overland flow and this similar subsurface infiltration excess may in fact be the same processes based on the observed similarities. In this respect, soil acts as a delay to the development of patches of saturation. For both overland flow and subsurface stormflow, the networked pattern and connectivity of the saturated patches, and not the saturation at any one point, determine the flow threshold (and connected flow path) at the hillslope scale. But while the topographic surface controlling overland flow is readily observable, the subsurface boundary is much more difficult to characterize and may be subject to considerable vertical loss to underlying material [*Gabrielli et al.*, 2012; *Graham and McDonnell*, 2010; *Tromp-van Meerveld et al.*, 2007]. *McDonnell* [2013] has suggested that the continued focus on differentiation between overland flow and subsurface stormflow may be limiting innovation in how we conceptualize, and ultimately model, runoff generation. Exploring the similarities between overland flow and subsurface stormflow may be a useful means of supporting runoff process research which may aid improved process measurement, understanding, and prediction.

Past works have explored, to some extent, the issue of overland flow and subsurface stormflow similarity. *Beven* [1981, 1982] showed that a 1-D kinematic wave model is valid for the simulation of subsurface stormflow for certain ranges of slope angle and hydraulic conductivity. Later, *Sloan and Moore* [1984] showed that the efficacy of a 1-D kinematic wave model is comparable to a 2-D Richards-based model for subsurface stormflow simulation, except for the simulation of hydrograph recession. However, the idea that overland flow and subsurface stormflow follows the same kinematic wave theory was generally rejected by *Singh* [2001, 2002] who showed that the applicability of kinematic wave theory in the simulation of subsurface stormflow is highly dependent on the rate of recharge, soil hydraulic conductivity, slope angle, and the thickness of saturated zone.

Here we revisit some of these early discussions regarding the kinematics of overland flow and subsurface stormflow and test the *McDonnell* [2013] thesis by using an overland flow model to predict subsurface stormflow at the hillslope scale. We construct numerical experiments to investigate physical similarities between overland flow and subsurface stormflow. We use the well-studied Panola Mountain Research Watershed (PMRW) hillslope [*Freer et al.*, 2002; *Tromp-van Meerveld et al.*, 2008] as the basis for this set of numerical experiments. Past process work at the Panola [*Tromp-van Meerveld and McDonnell*, 2006a,2006b] has shown that there is no evidence of either infiltration excess or saturation excess overland flow on the Panola hillslopes nor any bedrock exfiltration into the soil from below. We use the fully integrated subsurface-surface flow model HydroGeoSphere (HGS) [*Therrien et al.*, 2008] as our model "ground truth" and simulate subsurface stormflow using the 3-D variably saturated Darcy-Richards subsurface flow model within HGS. Then after the "removal" of the soil mantle, subsurface stormflow along the soil-bedrock interface is simulated using a 2-D diffusion wave overland flow model where the physical removal of the soil is compensated for by using a Manning's Roughness coefficient; loss along the "overland flow path" is represented by infiltration into the bedrock layer below.

The main focus of this work is assessment of the similarities between variably saturated subsurface flow (VSSF) and overland flow (OF) models for routing subsurface stormflow near the soil-bedrock interface. To guarantee an equal input to the bedrock surface in both models, for OF model the seepage flux at the base of the topsoil calculated by the VSSF model is used as a direct input to the bedrock surface. We use a minimal calibration approach to develop both the VSSF and OF models. Our objective of model calibration is not to generate comprehensive models with the ability to represent the entirety of complex processes that have been observed at the Panola; rather, we focus on comparing the efficacy of the VSSF and OF models for the simulation of subsurface stormflow along the bedrock surface at the soil-bedrock interface. We then assess to what extent both VSSF and OF models can simulate the subsurface stormflow hydrograph by performing a series of virtual experiments [*Weiler and McDonnell*, 2004] to explore the impact of different slope and rainfall magnitudes on resulting lateral flow.

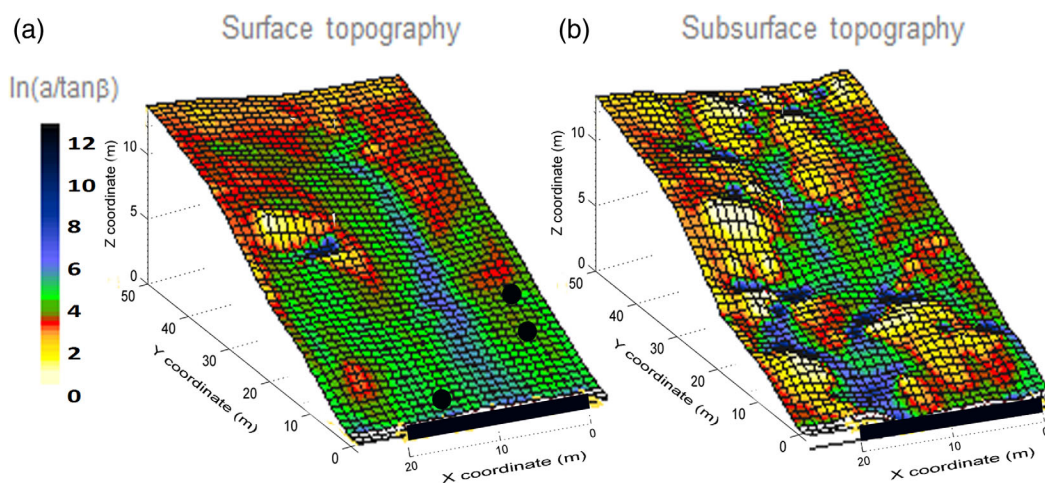


Figure 1. The layout and topographic index of the (a) surface and (b) bedrock topography. Excavated trench is shown in black. Black circles show the location of tensiometers used in model development. Figure developed originally by J. Freer, Bristol University.

We also use a simpler approach for handling soil seepage with the overland flow model as an alternative to the seepage calculated at the base of the soil by the VSSF model. In this simulation (OF_{prec}), the seepage at the base of the soil is approximated using a simple transfer function approach to delay and dampen the precipitation input signal. The transfer function is unit hydrograph approach as a proxy for the hydrological effect of the removed soil and to mediate the arrival of precipitation at the soil-bedrock interface; the precipitation transferred is then used as a direct input to the bedrock surface.

Specifically, we ask:

1. How well can the 2-D (friction and gravity based) overland flow model predict subsurface stormflow compared to a 3-D (capillarity and gravity based) variably saturated subsurface flow model?
2. To what extent overland flow and variably saturated subsurface flow models are similar in subsurface stormflow routing along the partitioning surface?
3. What is the role of the soil-bedrock interface in runoff partitioning with and without the presence of soil?
4. What can we learn about the role of the soil in runoff generation in forested hillslope?

2. Field Site

The study site used here is part of the PMRW, located 25 km southeast of Atlanta. The bedrock and surface topography generated from a 1 m DEM (described in detail in *McDonnell et al.* [1996] and then *Freer et al.* [2002]) are shown in Figure 1. The 20 m wide trench (in black) at the hillslope base collects lateral subsurface stormflow in 10 separate 2 m wide sections. Sink analysis within ArcGIS based on the 1 m DEM indicated that there are no pits or depressions that can store significant amounts of water along this (on average) 13% steep hillslope. The data used here, including long-term hydrometric data (e.g., pressure head, volumetric moisture content, lateral subsurface stormflow, rainfall), hillslope geometry, and hillslope material properties are described in detail in *Burns et al.* [1998], *Freer et al.* [1997], and *Tromp-van Meerveld et al.* [2008]. The competent granite bedrock in the Panola hillslope is overlain by a thin layer of saprolite and 0.63 m (on average) of sandy loam soil [*McIntosh et al.*, 1999; *Tromp-van Meerveld et al.*, 2007].

The original case study assessed here focused on the hillslope hydrologic response to a 95 mm rainstorm that occurred on 6–7 March 1996. In a manner similar to *Keim et al.* [2006], throughfall is considered over the hillslope for this rainfall event after subtracting the effect of canopy storage and evaporation from the canopy. Evapotranspiration during the event is neglected for this pregrowing season 2 day period. This event was preceded by a 7 day dry period; subsurface runoff had stopped and pressure heads were almost at steady state prior to the onset of the storm event. The average and maximum storm size reported at the Panola is 22 mm and 160 mm, respectively, and the threshold rainfall depth necessary to generate

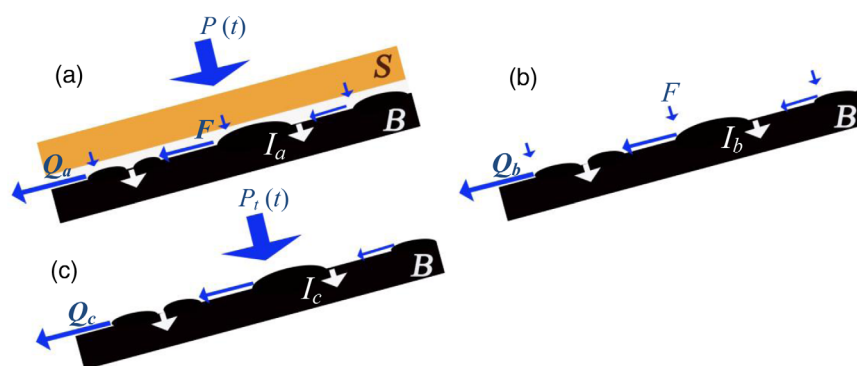


Figure 2. Conceptual models used in this paper. (a) Variably saturated subsurface flow (VSSF) model including soil (S) and thin transition sublayers underlined by competent bedrock (B). Uniform precipitation ($P(t)$) is imposed along the soil surface and $Q_a(x,y,z,t)$ and $I_a(x,y,z,t)$ represent the simulated subsurface stormflow and infiltration to the bedrock, and $F(x,y,z,t)$ represents the seepage at the base of the soil mantle. (b) Overland flow model (OF) including competent bedrock (B) while the vertical resistance of the removed sublayers are incorporated by imposing soil seepage $F(x,y,z,t)$ derived from model a, and $Q_b(x,y,z,t)$ and $I_b(x,y,z,t)$ represent the simulated subsurface stormflow and infiltration to the bedrock. (c) Overland flow model (OF_{prec}) including competent bedrock (B) with the removed soil sublayers, transferred precipitation ($P_t(t)$) is imposed along the soil bedrock interface and $Q_c(x,y,z,t)$ and $I_c(x,y,z,t)$ represent the simulated subsurface stormflow and infiltration to the bedrock. The bottom boundary of the computational domain is assumed to have a similar average slope as soil bedrock interface.

subsurface stormflow has been estimated at roughly 55 mm [Tromp-van Meerveld and McDonnell, 2006a]. The 6–7 March 1996 rainstorm used here is above this threshold for hillslope subsurface stormflow activation.

3. Numerical Experiments

3.1. Method

Similarities between runoff forms were assessed through separate simulations of subsurface stormflow using variably saturated subsurface flow (Darcy-Richards' equation) and overland flow (diffusion wave equation) models. The computer code used here for both simulations is contained within HGS which has been designed to simulate 2-D overland flow and 3-D subsurface flow using a fully coupled approach. Figure 2 shows a schematic representation of the models used in this paper. Using the VSSF approach (Figure 2a), we develop a model that is consistent with tensiometer pressure head observations and lateral subsurface flow at the trench face, collected for the 6–10 March 1996. This model includes three layers: competent bedrock, a 10 cm transition layer located immediately above the competent bedrock at the base of the soil profile, and the soil layer above. The spatial and temporal distribution of seepage flux at the base of the soil, $F(x, y, z, t)$, generated from the VSSF model, was used in the OF model as the “input term” to the bedrock surface (Figure 2b). An alternative, simpler, overland flow approach was additionally considered where the overland flow model was used to simulate subsurface stormflow routing along the bedrock in response to the transferred precipitation (instead of the seepage generated through the soil from VSSF) as the input term to the bedrock surface (Figure 2c). A simple transfer function approach based on the Nash [1959] unit hydrograph scheme was used to approximate the mediation (delaying) effect of the removed soil. This model is termed as OF_{prec} while the original overland flow model with calculated soil seepage by VSSF model as a direct input to the bedrock surface is simply termed as OF in the remainder of this paper.

Overland flow was modeled with HGS using a diffusion wave approximation of the Saint-Venant equations. The overlying soil and thin transition layer were completely removed in this mode and resistance to flow is controlled solely by a surface roughness parameter (Manning coefficient). The Manning coefficient [Manning *et al.*, 1890] is an empirically derived coefficient, which is dependent on surface roughness and surface cover. Here this coefficient was calibrated to lateral subsurface flow at the trench face in the OF model. This coefficient compensates for the removed soil in the overland flow model development phase. All the remaining model elements in the diffusion wave model, including bedrock geometry, bedrock material properties, bedrock initial and boundary conditions, were identical to those used in the Darcy-Richards model. In the OF_{prec} model, also a same Manning coefficient as the OF model was used without further calibration.

Figure 2 also depicts schematically the simulated infiltration to the bedrock ($l(x, y, z, t)$), and subsurface stormflow ($Q(x, y, z, t)$) using the three approaches (i.e., VSSF, OF, and OF_{prec}). The VSSF and OF models were then used to investigate the extent to which they are similar vis-à-vis subsurface stormflow simulation. Using virtual experiments, different hypothetical bedrock slopes (6.5% and 26%) and rainfall depths (65 and 190 mm) were considered to assess the potential similarities between the performances of two models. We note that the maximum observed rainfall depth at the Panola is 160 mm. The remaining model parameters (bedrock and soil material properties and soil depth) were fixed based on field measurements and calibrated parameters in the base case. Note that by considering identical soil depth distribution for various bedrock slopes we are able to isolate the effect of bedrock slope in runoff routing and not confound the effect of slope.

We use the Nash Sutcliffe measure [Nash and Sutcliffe, 1970] to assess the goodness of fit between simulated results (Q_a, Q_b, Q_c) and observed hydrograph. Furthermore, we apply two nonparametric tests, to assess whether or not OF and VSSF models are actually similar in predicting subsurface stormflow hydrograph and infiltration to the bedrock time series. Levene's [Olkin, 1960] and Kolmogorov-Smirnov [Massey, 1951] tests check if the variances and the cumulative distribution functions (CDFs) of the hydrographs obtained from two models are statistically similar. Indeed, our null hypothesis is that both OF and VSSF models predict an equal variance of the hydrograph (or bedrock infiltration time series) and probability of occurrence of flow (or bedrock infiltration) magnitudes. The decision to reject or accept the null hypotheses is based on comparing the p values with the significance level. We refer to Modarres [2010] for a general discussion of statistical tests used to assess the potential similarities between different hydrological models. Here we use a significance level of 0.05. At any p value larger than the significance level, we accept the null hypothesis.

3.2. Mathematical Formulation

HydroGeoSphere (HGS) uses a control volume finite element method to simultaneously solve the subsurface and overland flow equations. Richards' equation is used to describe 3-D transient subsurface flow in a variably saturated porous medium:

$$\frac{\partial}{\partial x} \left(K_{px} \frac{\partial h_p}{\partial x} \right) + \frac{\partial}{\partial y} \left(K_{py} \frac{\partial h_p}{\partial y} \right) + \frac{\partial}{\partial z} \left(K_{pz} \frac{\partial h_p}{\partial z} \right) + \Gamma \pm Q_p = \frac{\partial \theta}{\partial t} \quad (1)$$

where θ [-] is water content, K_{px} , K_{py} and K_{pz} [LT^{-1}] are porous media hydraulic conductivities, h_p [L] is porous media total hydraulic head, Γ [T^{-1}] is fluid exchange per unit volume between subsurface and surface domains, and Q_p [T^{-1}] is a volumetric fluid flux per unit volume representing an external source (positive) and sink (negative).

A simplified version of the 2-D depth-integrated Saint-Venant equations is used for the simulation of transient overland flow. In the complete form, the 2-D depth-integrated Saint-Venant equations include a mass balance equation:

$$\frac{\partial}{\partial t} (\varnothing_o h_o) + \frac{\partial}{\partial x} (d_o \bar{v}_{x_o}) + \frac{\partial}{\partial y} (d_o \bar{v}_{y_o}) + d_o \Gamma \pm Q_o = 0 \quad (2a)$$

momentum equation in the x direction:

$$\frac{\partial}{\partial t} (d_o \bar{v}_{x_o}) + \frac{\partial}{\partial x} (d_o \bar{v}_{x_o}^2) + \frac{\partial}{\partial y} (d_o \bar{v}_{x_o} \bar{v}_{y_o}) + g d_o \frac{\partial (d_o)}{\partial x} - g d_o (S_{ox} - S_{fx}) = 0 \quad (2b)$$

and momentum equation in the y-direction:

$$\frac{\partial}{\partial t} (d_o \bar{v}_{y_o}) + \frac{\partial}{\partial y} (d_o \bar{v}_{y_o}^2) + \frac{\partial}{\partial x} (d_o \bar{v}_{x_o} \bar{v}_{y_o}) + g d_o \frac{\partial (d_o)}{\partial y} - g d_o (S_{oy} - S_{fy}) = 0 \quad (2c)$$

where \varnothing_o [-] is a surface flow domain porosity (for definition, see Frei and Fleckenstein [2014] and Therrien et al. [2008]), h_o is water surface elevation [L], d_o is the depth of surface flow [L], and Q_o [LT^{-1}] is a volumetric flow rate per unit area representing an external source (positive) or sink (negative). S_{ox} , S_{oy} , S_{fx} , and S_{fy} are dimensionless bed and friction slopes in x and y directions, respectively. Depth-averaged velocities in x and y directions are \bar{v}_{x_o} and \bar{v}_{y_o} [LT^{-1}]. Equations (2b) and (2c) are simplified in HGS by neglecting local and convective inertia terms (the first three terms on the left side). Then, using Manning friction slope equations:

$$S_{fx} = \frac{\bar{v}_{xo} \bar{v}_{so} n_x^2}{d_o^{\frac{4}{3}}} \quad (3a)$$

$$S_{fy} = \frac{\bar{v}_{yo} \bar{v}_{so} n_y^2}{d_o^{\frac{4}{3}}} \quad (3b)$$

Equations (2b) and (2c) are simplified to

$$\bar{v}_{xo} = -K_{ox} \frac{\partial h_o}{\partial x} \quad (4a)$$

$$\bar{v}_{yo} = -K_{oy} \frac{\partial h_o}{\partial y} \quad (4b)$$

$$K_{ox} \approx \frac{d_o^{\frac{2}{3}}}{n_x} \text{ and } K_{oy} \approx \frac{d_o^{\frac{2}{3}}}{n_y}$$

where \bar{v}_{so} is the depth-averaged velocity [LT^{-1}] along the direction of maximum slope. In addition, K_{ox} and K_{oy} [LT^{-1}] are the surface conductances, and n_x and n_y [$L^{-1/3}T$] are the Manning roughness coefficients in x and y direction, respectively. The overland flow equation implemented by HGS is then obtained by substituting the momentum equations (i.e., equations (4a) and (4b)) into the mass balance equation (equation (2a)), leading to the 2-D diffusion wave equation:

$$\frac{\partial}{\partial x} \left(d_o K_{ox} \frac{\partial h_o}{\partial x} \right) + \frac{\partial}{\partial y} \left(d_o K_{oy} \frac{\partial h_o}{\partial y} \right) - d_o \Gamma \pm Q_o = \frac{\partial}{\partial t} (\varnothing_o h_o) \quad (5)$$

Subsurface-surface coupling is implemented using a dual node approach that defines, Γ , the fluid exchange per unit volume between subsurface and surface domains. The dual node approach uses a computational parameter referred as the "coupling length" (l_{ex} [L]) to facilitate the computation of exchange between surface and subsurface continua as:

$$\Gamma = \frac{K_{pz}}{d_o l_{ex}} (h_p - h_o) \quad (6)$$

In the overland flow modeling approach used here surface and subsurface continua are the zones above and below the soil-bedrock interface. To ensure a proper implementation of the exchange between subsurface and surface domains a small coupling length is required; this in turn increases the computational cost [Liggett et al., 2012]. Liggett et al. [2012] suggested a value of $l_{ex} \ll 10^{-2}$ m for infiltration under infiltration excess conditions. We use a value of 10^{-4} m in this paper. It is interesting to note that the governing equations for both VSSF and OF models are mathematically similar (equations (1) and (5)). Both are derived based on conservation of mass and some approximation of the momentum equation. In this paper, we assess and demonstrate the application of these similarities in the case of Panola.

Numerical models based on the standard Saint-Venant equation may be subject to instability and convergence issues. This is especially true for simulation of shallow overland flow over steep surfaces with irregular topography and sharp wet-dry transitions [e.g., Costabile et al., 2012]. In addition, the simulation of coupled subsurface-surface models with a reasonably small coupling length (equation (6)) would be computationally inefficient when the standard 2-D Saint-Venant equation is used (equation (2)). Simplified versions of the standard Saint-Venant equation, i.e., diffusion wave and kinematic wave equations are widely used in the simulation of 1-D and 2-D shallow overland flow. These equations can properly emulate the behavior of full Saint-Venant equation where local and/or convective inertial effects (which are represented by the first three terms of equations (2b) and (2c)) are sufficiently small compared to the effect of pressure gradient, slope, and friction (which are represented by the fourth and fifth terms of equations (2b) and (2c)) [Almeida and Bates, 2013; Kazezyilmaz-Alhan and Medina, 2007]. Although both equations ignore inertial effects, the kinematic wave equation additionally ignores the pressure gradient effect (the fourth term in equations (2b) and (2c)). The pressure gradient term describes the spatial variability of water pressure head, and since the pressure is assumed hydrostatic, this term represents the spatial variability of OF depth.

We here assess the effect of ignoring local and/or convective inertia and pressure gradient terms by calculating their magnitude in the full Saint-Venant equation (equation (2)). We then use the relative magnitude

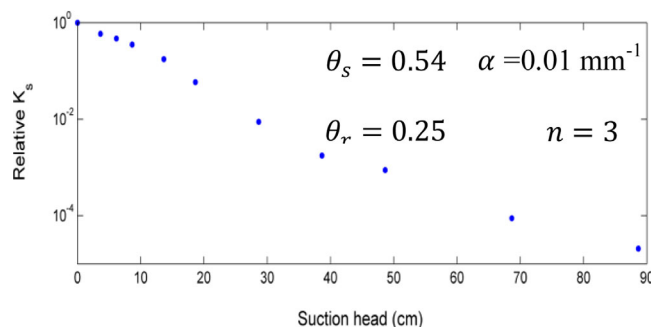


Figure 3. Soil water characteristic curve of the sandy loam soil used here. This was obtained based on lab test on soil cores taken from Panola [Tromp-van Meerveld et al., 2008]. α and n are fitted van Genuchten parameters.

prism elements and 27,783 nodes in 20 sublayers, was set up using the preprocessor GridBuilder [McLaren, 2004] and HGS to generate the computational domain. The surface and bedrock topography (Figure 1) of the Panola hillslope was imported from the 1 m resolution DEM over the 28 by 50 m study area. In the model development phase, soil unsaturated material properties were determined solely from direct observation. It is known that, in variably saturated flow simulation, subsurface flow is highly sensitive to the soil water characteristic curve [Ebel et al., 2010; Loague et al., 2010]. We determined soil water characteristic curve from soil cores taken directly from the Panola hillslope at different depths (Figure 3) (as reported in Tromp-van Meerveld et al. [2008]).

The initial condition in the soil mantle was also determined from direct observation at the Panola. This is different to previous modeling work at the Panola [Hopp and McDonnell, 2009, 2011; Keim et al., 2006] where uniform initial moisture conditions were assumed. Available tensiometer data at the study site (at 12 Am, on 6 March 1996) indicated pronounced heterogeneity in the soil initial moisture condition. At the Panola, Keim et al. [2006] reported the uniformity of initial soil moisture condition assumption as a possible source of error in model calibration phase. To incorporate this heterogeneity, available tensiometer pressure head data at 44 locations were interpolated using a nine term 3-D Fourier series to represent initial pressure head at all nodes of the soil layer.

We calibrated the VSSF model to match both transient tensiometer data and flow at the trench face using initial conditions and saturated and unsaturated material properties of the underlying granite bedrock and thin transition layer, in addition to saturated hydraulic conductivity of the soil mantle. Table 1 shows the range of saturated hydraulic conductivities reported in the Panola from field and laboratory experiment by, e.g., Appels et al. [2015], McIntosh et al. [1999], Tromp-van Meerveld et al. [2007, 2008], and White et al. [2002].

In a manner similar to Hopp and McDonnell [2009], the upslope boundary and the sides of the domain were treated as no-flow conditions. Further, the entire width (28 m) of the downslope hillslope boundary (including the location of excavated trench face) was treated using a seepage face boundary condition along the soil and thin transition sublayers, with a no-flow condition along the competent bedrock. It is important to note that the simulated subsurface trench flow that is reported in this paper originates only from the nodes that correspond to the location of the 20 m wide trench excavated downslope of the hillslope (Figure 1). A unit vertical hydraulic gradient (free drainage) boundary condition was assigned along the bottom boundary of the bedrock. This boundary was represented by an inclined base parallel to soil-bedrock interface (Figure 2). This treatment of the bottom boundary interface aided in the consistent comparison between various slopes of soil-bedrock interface. Using this scheme, the thickness of the bedrock and more importantly the mesh discretization for all simulations with different bedrock slopes was identical. Across the surface of the modeled domain, hourly throughfall rates (hourly measured precipitation was modified by incorporation of canopy storage and canopy evaporation following Keim et al. [2006]) were applied (Figure 2a).

3.4. Overland Flow Model (OF and OF_{prec})

To simulate subsurface stormflow along the bedrock interface using the overland flow approach, the soil layer and thin transition layer were removed. As illustrated in Figure 2b, in the OF model the seepage flux

of each term to rigorously justify the use of the diffusion wave approximation for simulation of subsurface stormflow at the Panola. We assumed additionally a subcritical flow regime along the bedrock in the OF model. Froude numbers corresponding to velocities along the bedrock for different examples considered in this paper are used to assess the validity of this subcritical flow assumption.

3.3. Variably Saturated Subsurface Flow (VSSF) Model

A 3-D mesh including 49,920 triangular

Table 1. Range of Soil and Bedrock Saturated Hydraulic Conductivities Reported From Field and Lab Experiment in the Panola

Material	k_s (mm h ⁻¹)
Sandy loam soil	576–648
Competent granite	1.44–14
Transition layer	$\frac{316^a}{15}$

^aAverage of measurements immediately above the bedrock reported by Appels *et al.* [2015], top and bottom values represent lateral and vertical hydraulic conductivities, respectively.

distribution from the base of the soil generated by the VSSF model, ($F(x, y, z, t)$), was applied over the bedrock interface. The bedrock surface was initialized with a zero flow depth. To allow overland flow to exit at the edges of the domain, a critical depth boundary condition (free overfall) was imposed along the surface boundaries of the bedrock. This treatment is consistent with the subcritical flow assumption used here. Manning’s coefficient was obtained using a simple manual calibration of the simulated subsurface stormflow hydrograph ($Q_b(x, y, z, t)$) to the observed trench flow hydrograph. To account for infiltration to the bedrock, a coupling length (equation (6)) of 10^{-4} m was used. This value was chosen two order of magnitude smaller than the threshold value proposed by Ebel *et al.* [2009] and Liggett *et al.* [2012] to ensure a realistic coupling between flow over bedrock interface and competent bedrock, and accurate treatment of infiltration to the bedrock ($I_b(x, y, z, t)$ in Figure 2b).

In the OF_{prec} model, the transferred precipitation (P_t) was directly applied over the bedrock (Figure 2c) instead of the seepage at the base of the soil generated by VSSF model, while other parameters (variables) including the Manning’s coefficient were assumed to be the same as the original OF model.

To calculate the transferred precipitation from real precipitation (P), the unit hydrograph approach proposed by Nash [1959] was used as:

$$P_t(t) = P(t) * UH(t) \tag{7}$$

where $UH(t) = \frac{1}{i(j-1)!} e^{-\frac{t}{i}} \left(\frac{t}{i}\right)^{(j-1)}$

The asterisk (*) represents the convolution operation, and i and j are the scale and shape parameters of the model. These parameters represent the delaying behavior of the removed soil. Here a fixed shape parameter of 4 (as has done in Clark *et al.* [2008]) is considered while the scale parameter is approximated (calibrated) as 0.75 h based on the observed rainfall-runoff during the study period.

4. Results

4.1. Calibration of the Variably Saturated Subsurface Flow (VSSF) Model

VSSF model parameters were manually calibrated to match pressure head time history of two tensiometers (16-1 S and 2-13 D) and the observed trench flow hydrograph. Data from other tensiometers were reserved for the validation of the model. Calibrated parameters are listed in Table 2. In this table, k_s refers to the saturated hydraulic conductivities which are listed in x , y , and z directions.

Table 2 shows the calibrated saturated hydraulic conductivities for three sublayers. Sandy loam soil and competent granite layers are largely isotropic. However, the downslope and vertical hydraulic conductivities of transition layer were 720 mm h^{-1} and 18 mm h^{-1} , respectively, which suggests some anisotropy. This reflects the high lateral conductivity and anisotropy for the transition layer compared to the soil and bedrock. Appels *et al.* [2015] reported a high downslope hydraulic conductivity immediately above the bedrock with an average of 316 mm h^{-1} , and a maximum of 1995 mm h^{-1} . These measurements were obtained based on falling head test data from 135 wells located at the soil-bedrock interface. The downslope conductivity of this zone was higher than the soil mantle and competent bedrock conductivities measured based on Guelph permeameter and sprinkling experiments, respectively. In addition, they demonstrated that deep soil vertical hydraulic conductivity (in the vicinity of the soil-bedrock interface) was on the order of 15 mm h^{-1} . Large lateral conductivity and high anisotropy of the layer immediately above the bedrock may be associated with shallow bedrock geology with connected fractures parallel to land surface produced by exfoliation [Tromp-van Meerveld *et al.*, 2007]. These measurements motivate the hydraulic conductivities and high anisotropy used here for the thin transition layer located immediately above the competent bedrock.

Table 2. List of Calibrated Parameters in Variably Saturated Model Development Phase^a

Material	k_s (mm h ⁻¹) ^b	θ_r	θ_s	α (mm ⁻¹)	n	Initial Saturation (%)
Sandy loam soil	635, 635, 640					
Transition layer	200, 700, 18 ^c	0.06	0.20	0.001	2.25	60
Competent granite	1.8, 1.8, 1.5	0.01	0.06	0.001	2.75	72.5

^aThe initial saturation percentage is the parameter used by HGS to represent the percentage of saturated moisture content assigned as an initial condition. Unsaturated properties and initial condition of sandy loam soil were considered based on lab test on soil cores (Figure 3) and observed initial pressure head for the event.

^bOrdered in x, y, and z direction, respectively.

^cDownslope saturated hydraulic conductivity would be equal to 720 (mm h⁻¹) based on 13% slope.

Comparisons between the simulated and observed pressure heads at the four tensiometer locations are shown in Figure 4. Even with fixed soil unsaturated hydraulic parameters, Nash Sutcliffe [Nash and Sutcliffe, 1970] values (NS) for calibration were 0.51 and 0.31 (Figure 4a). Nash Sutcliffe values of validation phase were 0.19 and 0.18 for tensiometers 2-9 S and 16-1 D (Figure 4b) while for the remaining tensiometers this measure was smaller. This indicates that at some locations, the model performance with respect to matric potential simulation did not properly match the observations. This disagreement, to some extent, can be attributed to the arrangement of nodes in mesh layers; there was not always a node at exactly the required depth to match the tensiometer cups. Furthermore, some of the discrepancies between observed and simulated matric potential during peak flow can be tied to the laboratory estimation of soil characteristic curve parameters, which usually is determined under drying and not wetting conditions [Mirus, 2015]. Additionally, the initial portion of the simulation involves some redistribution and immediate drainage lead to poor model performance of VSSF model at early times. Some warm up simulation (as has done, e.g., by Mirus et al. [2007]) was able to mitigate this error. However, as noted earlier, in the original comparison made in this paper the VSSF model (which was calibrated with fixed soil unsaturated hydraulic parameters) is only intended to be compared with the OF model where the bedrock properties and seepage over the bedrock are the same for both models. In other words, the objective of this model development

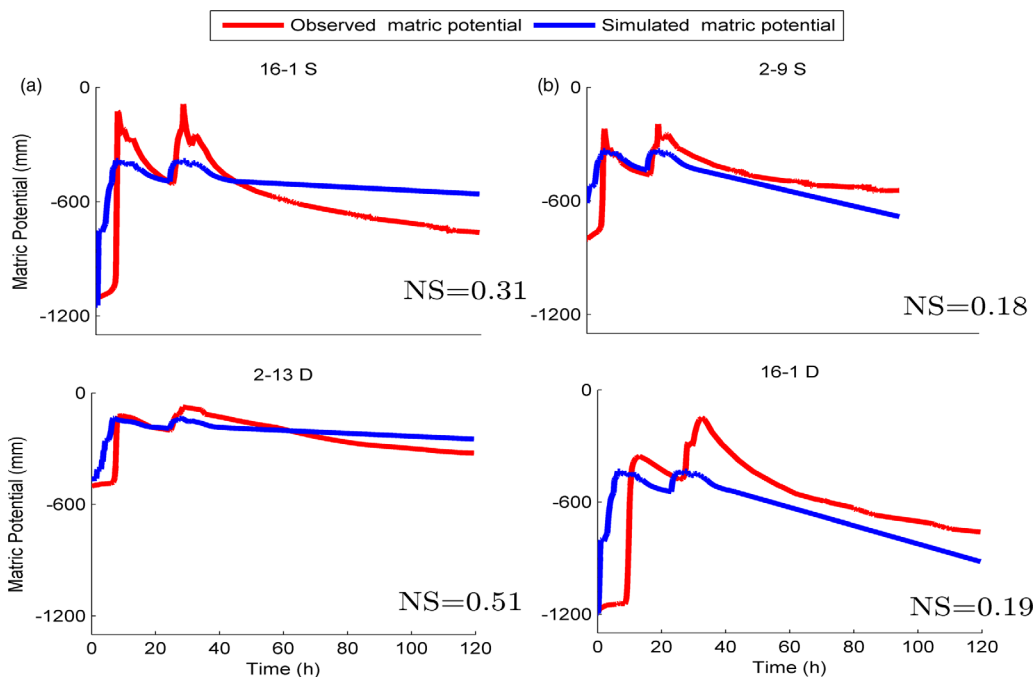


Figure 4. Performance of the variably saturated subsurface flow model (VSSF) with respect to matric potential, (a) comparison between observed and simulated pressure heads at tensiometers (16-1 S, 2-13 D) in the model calibration phase. These two tensiometers bracketed the tensiometer field on the hillslope as reported in Freer et al. [2002] and were specifically chosen here to represent the full extent of the measured area. (b) Comparison between observed and simulated pressure heads at tensiometers (2-9 S, 16-1 D) in validation phase. Tensiometers are named according to their locations where the digits represent x and y coordinates, respectively, and S and D indicate the tensiometer depth (Shallow and Deep; approximately 20 cm and 59 cm, respectively).

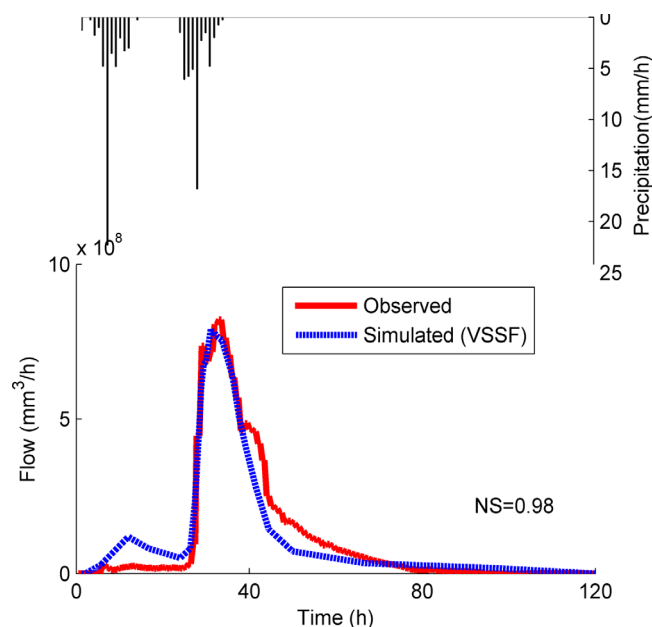


Figure 5. Performance of the variably saturated subsurface flow (VSSF) model with respect to observed trench flow in the model calibration phase.

was not to build a model that exactly emulates all of the complex flow processes that have been observed at the Panola.

The VSSF model is able to simulate subsurface stormflow hydrograph at the trench face (Figure 5) with a Nash Sutcliffe value of $NS = 0.98$ between simulated and observed trench flow. Simulated hydrograph shows that the major stormflow is activated 27.5 h after the start of precipitation; peak and recession flow are also occurred at $t = 31.5$ h and $t = 36$ h, respectively. The runoff coefficient after 5 days simulation period for the VSSF model was 8.5%; the measured runoff coefficient for this event was 10%. Here the runoff coefficient is defined as the ratio between cumulative subsurface stormflow depth collected (or simulated) in the trench and precipitation depth.

4.2. How Well Can an Overland Flow Model Predict Subsurface Stormflow?

4.2.1. Subsurface Stormflow Hydrograph

Figure 6 shows the simulated results of the subsurface stormflow at the soil-bedrock interface using the overland flow modeling approaches. In the OF model, using a simple manual calibration of simulated subsurface stormflow hydrograph ($Q_b(x, y, z, t)$ in Figure 2b) to observed trench flow hydrograph, a Manning coefficient of $n = 16 \text{ s m}^{-1/3}$ was obtained with a Nash Sutcliffe value of $NS = 0.95$. Note that the Manning coefficient compensates for the absence of soil and absence of the thin transition sublayers in the OF model. The typical value of Mannings coefficient for open channel flow with a mild vegetation cover is less than 0.5. However, here it is a surrogate for the high resistance provided by porous media, rather than vegetation, and may therefore be expected to exceed this upper value for open-channel flows. Similar to the observed hydrograph, the simulated hydrograph shows that the major stormflow pulse is activated 27.5 h after the start of precipitation; peak and recession flows occurred at $t = 35.5$ h and $t = 36$ h, respectively. The runoff coefficient after the 5 day simulation period for overland flow model was 7.5%. Simulated subsurface stormflow hydrographs using the VSSF model, $Q_a(x, y, z, t)$, and the observed trench flow hydrograph at the Panola are also shown in Figure 6 for comparison purposes. The nonparametric tests suggest that there is no difference in the variance and cumulative probability of flow magnitudes between the OF and VSSF models hydrographs (Table 3). The Leven and Kolmogorov-Smirnov p values (0.93 and 0.345) were larger than the significance level (0.05) which implies that the null hypotheses (i.e., equality of variance and cumulative distribution function) were true. The cumulative distribution functions also suggest that both models similarly predict the probability and magnitude of high flow, medium flow, and low flow.

In spite of an overall acceptable goodness of fit between two models, they do not match one another exactly. This likely stems from the differences between two models in the fine details along the slope. For instance, in the overland flow approach the water pressure would be positive as soon as patches of saturation are generated (i.e., when infiltration excess occurs). There might be a negative pressure, however, along the bedrock using the VSSF model even after generation of patches of saturation due to the capillary effect. Additionally, patches of saturation are connected by capillary-based and friction-based mechanisms in VSSF and OF models, respectively.

The developed overland flow model then was used (without further calibration) to simulate subsurface stormflow routing along the bedrock, but this time with the transferred precipitation (P_t) as direct input to the bedrock surface ($Q_c(x, y, z, t)$ in Figure 2c). Figure 6 shows the simulated subsurface stormflow using

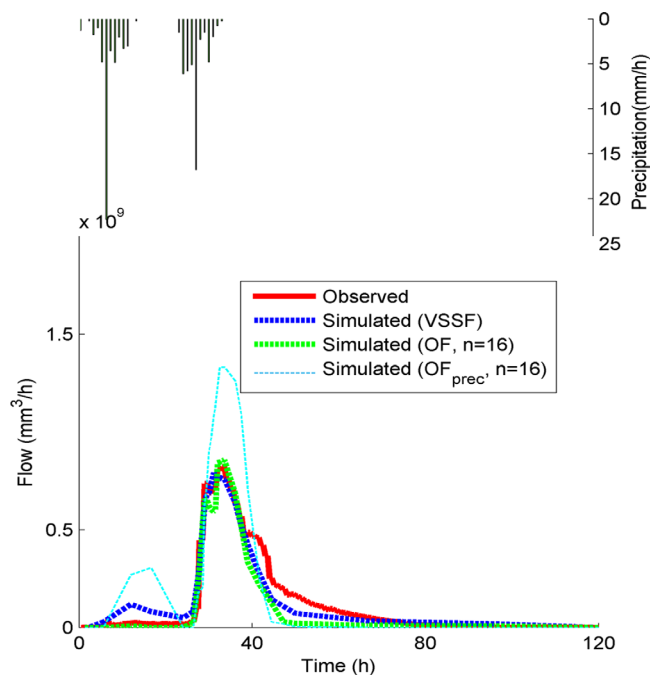


Figure 6. Comparison between overland flow models (OF and OF_{prec}) and variably saturated subsurface flow (VSSF) simulated hydrographs with observed trench flow.

were larger than the significance level so that we accept the null hypothesis. Indeed, there is no difference between OF and VSSF models in the prediction of variance of bedrock infiltration time series and the probability of occurrence of bedrock infiltration magnitudes. Although Figure 7a illustrates the spatially averaged infiltration flux into the bedrock and soil seepage over the bedrock, OF, OF_{prec} , and VSSF approaches suggest significant spatial variability in bedrock infiltration and soil seepage (not shown here).

Figure 7b indicates the cumulative seepage flow (mm) at the base of the soil (over the bedrock) and the cumulative infiltrated flow into the bedrock from both modeling approaches. Both OF and VSSF models show that until $t = 26.5$ h (1 h before major flow activation at $t = 27.5$ h), almost 70% of total soil seepage flow from the base of the soil has been infiltrated into the bedrock. In general, for the 6–7 March rainstorm, the bedrock recharge coefficient (defined as the ratio between bedrock infiltration and precipitation) is 79% and 80% for VSSF and OF models, respectively. These values are significantly larger than the modeled and observed runoff coefficients. Figure 7 also shows that the OF_{prec} model (with transferred precipitation as direct input to bedrock surface) can reasonably approximate the time history of bedrock infiltration obtained using VSSF model. Between VSSF and OF_{prec} models, the Leven and Kolmogorov-Smirnov p values (0.545 and 0.185) were larger than the significance level; therefore we accept the null hypothesis that there is no difference between OF_{prec} and VSSF models in the prediction of variance of bedrock infiltration time series and the probability of occurrence of bedrock infiltration magnitudes. The bedrock recharge coefficient obtained from the OF_{prec} model is also 83%.

Table 3. Results of Nonparametric Levene and Kolmogorov-Smirnov Tests Used to Assess the Similarities in Variance and Cumulative Distribution Functions Between VSSF and of Models^a

Test Case	Levene	Kolmogorov-Smirnov
Original	0.930	0.345
6.5% Slope	0.001	0.045
26% Slope	0.060	0.330
65 mm rainfall	0.430	0.190
190 mm rainfall	0.850	0.340

^aOriginal case is the test used in the model development phase (sections 4.1 & 4.2). The remaining test cases used in virtual experiment analyses (section 4.3).

OF_{prec} model can reasonably approximate the timing of the observed hydrograph with a Nash Sutcliffe value of $NS = 0.35$. The runoff coefficient was also obtained as 13% which is a reasonable approximation to the measured runoff coefficient for this event (10%).

4.2.2. Role of the Partitioning Boundary (Soil-Bedrock Interface)

4.2.2.1. Bedrock Infiltration

Figure 7a depicts the time history of spatially averaged simulated bedrock infiltration flux ($\bar{I}_a(t)$, $\bar{I}_b(t)$, and $\bar{I}_c(t)$) using variably saturated subsurface flow and both overland flow approaches (without further calibration). This figure also shows the spatially averaged seepage flux at the base of the soil, $\bar{F}(t)$, derived from the VSSF model, and uniform precipitation and the transferred precipitation time history. Again, between VSSF and OF models, the Leven and Kolmogorov-Smirnov p values (0.845 and 0.325)

4.2.2.2. Spatial Distribution of Sub-surface Stormflow

Figure 8 shows the observed and simulated spatial distribution of lateral subsurface stormflow along the trench using VSSF and OF models. The spatial distribution was not used as a calibration target; results are the direct by-product of the calibration discussed in sections 4.1 and 4.2. Four snapshots in

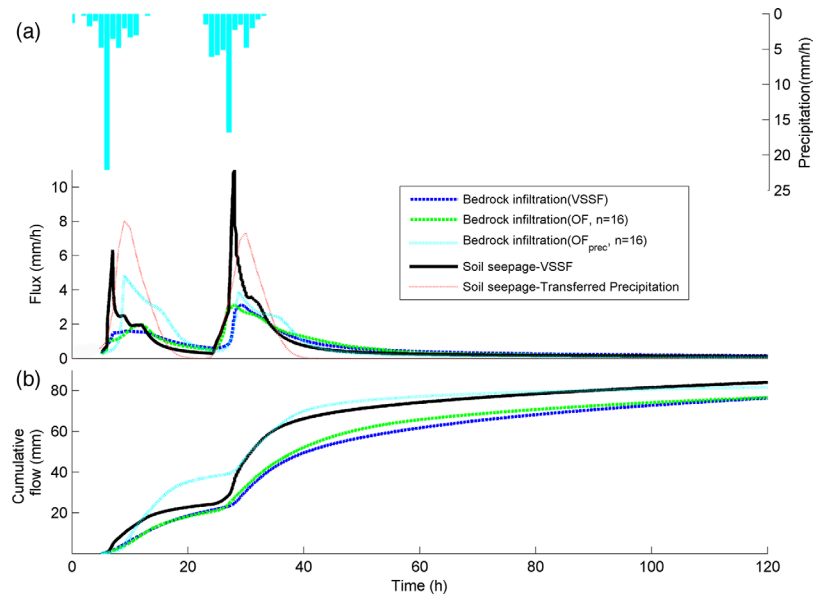


Figure 7. Simulated infiltration into the bedrock, (a) time history of spatially - averaged simulated infiltration flux into the bedrock from three approaches used here, along with seepage at the base of the soil calculated from VSSF (in black color), uniform precipitation and transferred precipitation (in light red color). (b) time history of cumulative flow over and across the bedrock.

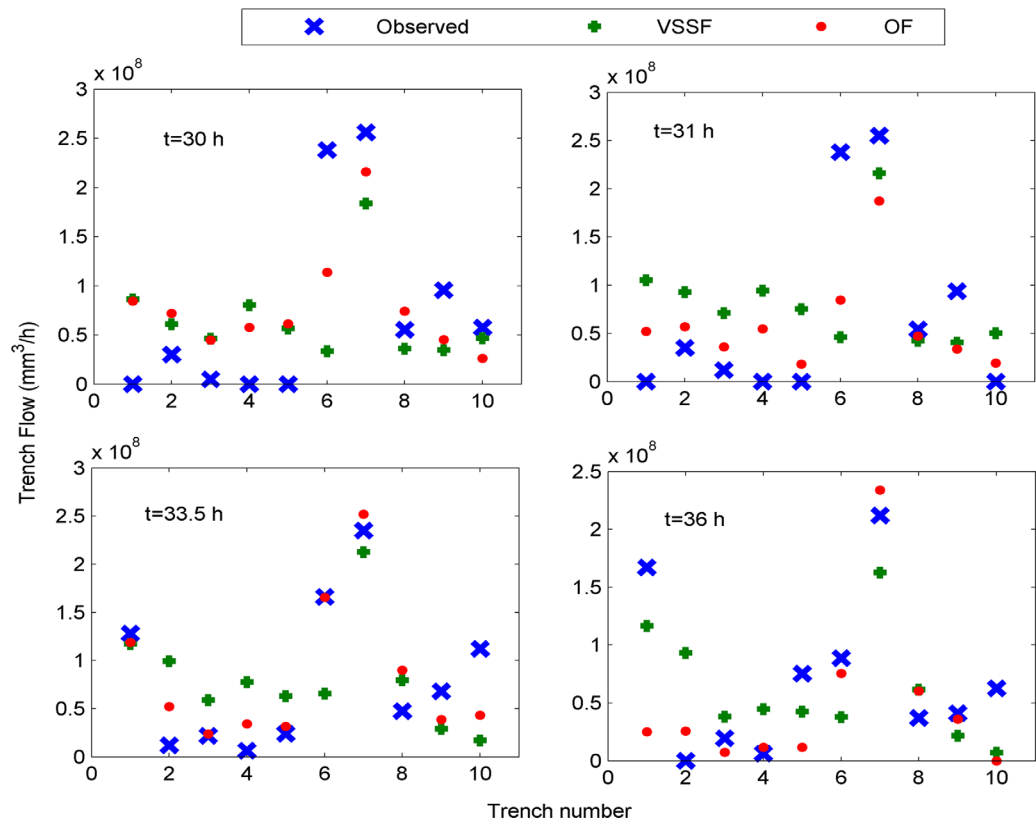


Figure 8. Observed and simulated (VSSF and OF approaches) spatial patterns of subsurface stormflow along the trench face at 4 different time steps during peak flow.

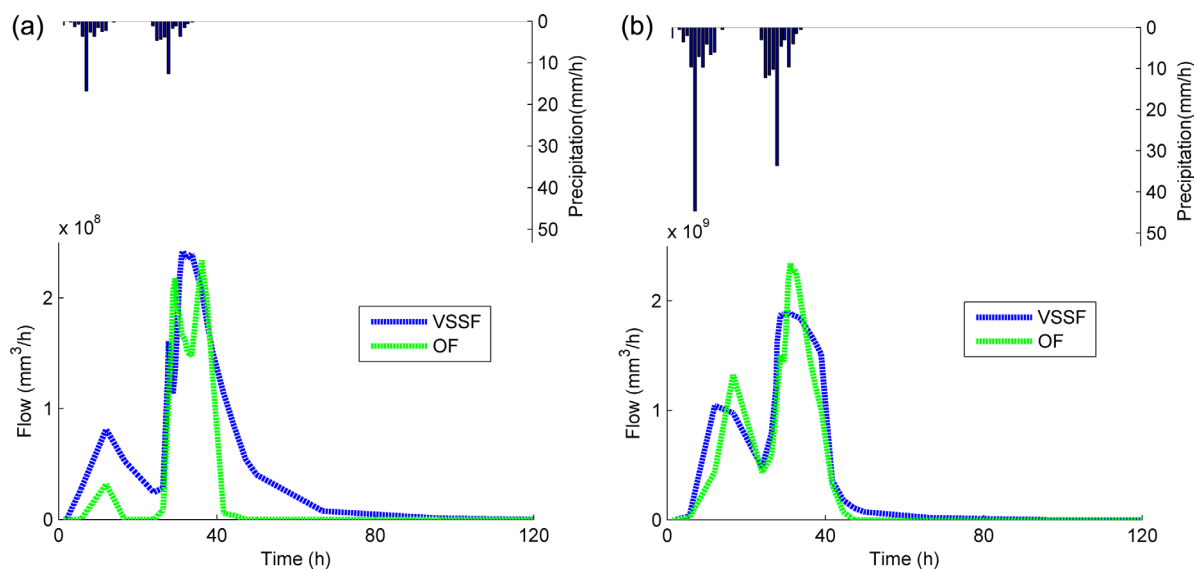


Figure 9. Comparison between OF and VSSF simulated hydrographs for two rainfall events. (a) 65 mm and (b) 190 mm.

time during the rising limb, flow peak and flow recession are shown (all values were obtained by accumulating the flow in a 2 m wide trench section with a total of 10 sections).

Like the early observational work at the site [McDonnell *et al.*, 1996] both VSSF and OF models show generally that most of the subsurface stormflow at the trench face appears between sections 6 and 8 (12 m < x < 16 m); consistent with the accumulated flow pattern along the Panola soil-bedrock interface [Freer *et al.*, 2002; McDonnell *et al.*, 1996] as shown in Figure 1b. Note that accurate estimation of the actual geometric boundaries of each trench section can be difficult. Therefore, perfect duplication of the spatial distribution of trench flow from all three schemes was not expected.

4.3. To What Extent Are the VSSF and OF Models Similar?

4.3.1. Effect of Rainfall Depth

Figure 9 compares the efficacy of the OF and VSSF models for simulation of Panola hillslope hydrologic response to 65 and 190 mm rainfall events. The depths of these two hypothetical events are 0.75 and 2 times larger than the original case study with 95 mm rainfall. The model parameters and initial conditions were identical to those used in base case VSSF and OF models.

For the 190 mm event, the OF and VSSF models produced comparable hydrographs, with the Leven and Kolmogorov-Smirnov p values (0.85 and 0.34) each larger than the significance level (Table 3). This suggests that the model hydrographs are not statistically distinguishable. There is also not any discernible difference between the two models in the prediction of the probability and magnitude of high flows, medium flows or low flows. Comparison between the response hydrographs reveals that the OF model predicts flow activation, two major discharge flow peaks and flow recession in a similar fashion to VSSF model, though the event timing is not replicated perfectly. These discrepancies may reflect some parameter compensation for rainfall magnitude in the original model calibration. Cumulative runoff characteristics are more strongly supportive of the argument that VSSF and OF behaviors are comparable; the runoff coefficients of VSSF and OF models were both 14%, while the bedrock infiltration coefficients were 49% and 45%, respectively.

For the 65 mm event, the distinction between OF and the VSSF hydrographs is more pronounced, with the Leven and Kolmogorov-Smirnov equal to 0.43 and 0.19; nevertheless these values were still larger than significance level which again supports the null hypotheses. Again, cumulative measures are strongly linked: the simulated runoff coefficients are 3.7% and 2.5% and the bedrock infiltration coefficients are 85% and 83% for VSSF and OF models, respectively. Results obtained from both models in this section and the models developed in sections 4.1 and 4.2 suggest that as the rainfall depth increases, the runoff coefficients increase and bedrock infiltration coefficients decrease. Additionally, the correspondence between OF and

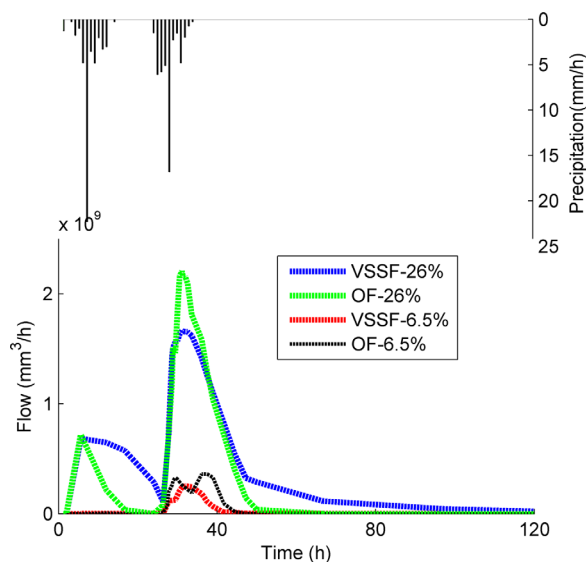


Figure 10. Comparison between OF and VSSF simulated hydrographs for two hypothetical bedrock slopes (6.5% and 26%).

VSSF models is improved. Both VSSF and OF models also indicate that there is no evidence of saturation excess overland flow and bedrock exfiltration even in response to 190 mm rainfall depth (which is 30 mm larger than the maximum rainfall depth observed in the Panola).

4.3.2. Effect of Slope

We performed a virtual experiment with VSSF and OF models (again, without any further calibration) to assess the effect of slope on similarities between OF and VSSF models. We used two different hypothetical bedrock slopes with an average of 6.5% and 26% to predict subsurface stormflow hydrograph (Figure 10). The bedrock topography was generated via rotation and scaling of the topographic surface from the base model. OF model was able to sufficiently mimic the VSSF stormflow hydrograph, for 26% slope of the bedrock. The Leven and Kolmogorov-

Smirnov p values (0.06 and 0.33) were larger than the significance level (Table 3) which suggests no significant differences between VSSF and OF models. The runoff coefficients of VSSF and OF models are 25% and 22%, respectively. The bedrock infiltration coefficients were 60% and 67% for VSSF and OF models. Compared to the base cases, these results suggest that as the slope increases from 13% to 26%, runoff coefficients increase almost by a factor of 3 while bedrock infiltration decreases. Additionally, both VSSF and OF models depict higher peak discharge values and earlier response times as slope increases.

For the 6.5% slope, both models indicate lower peak discharge values and later flow activation. Runoff coefficients were 1.8% and 2.3% for VSSF and OF models that were almost 4 and 3 times smaller than the coefficients from base case models. There was also an increase in bedrock infiltration coefficients compared to the base cases and the 26% bedrock. These bedrock coefficients were 88% and 94% for VSSF and OF models, respectively. Although the lumped characteristics (i.e., runoff and bedrock infiltration coefficients) were mimicked reasonably well by the OF model, the detailed behavior of subsurface flow hydrograph cannot be fully emulated by the OF model. The Leven p value was 0.001 (Table 3) which rejects the null hypothesis on the similarity of hydrograph variances between VSSF and OF models. The Kolmogorov-Smirnov p value was 0.045; this suggest a possible, but not significant, difference in the cumulative distribution functions of the flow magnitudes predicted by VSSF and OF models at the 0.05 significance level. For this gentle slope, the smaller gravitational influence on the hydraulic gradient may enhance the effect of soil compared to the original test case used in the calibration phase which has a steeper bedrock slope. Results, additionally depict a slow subsurface flow velocity along the bedrock (maximum simulated Froude number was 0.005) and low value of subsurface discharge at the trench (1.7 and 2.25 mm from VSSF and OF models). Therefore, the discrepancy between the VSSF and OF models may be related to the fact that the measureable subsurface stormflow does not occur along this gentle slope. Indeed, subsurface stormflow is characterized typically by rapid flow along the bedrock (or impeding layer) and significant trench flow discharge which is not the case for this example.

4.4. Effect of Soil on Runoff Generation in Forested Hillslopes?

Here we assess to what extent “soil” (i.e., the removed element in the overland flow models used here) is important in subsurface stormflow generation. This equates to: how much complexity is required to sufficiently represent the behavior of the topsoil? High resolution soil depth data comparable to the collected data at the Panola hillslope are generally not available for most hillslopes in either gauged or ungauged basins. To assess the effect of soil depth data resolution on subsurface stormflow response, we performed a virtual experiment with VSSF and OF models (again, without any further calibration). We used three different bedrock and soil surface resolutions including uniformly spaced measurements for the Panola hillslope

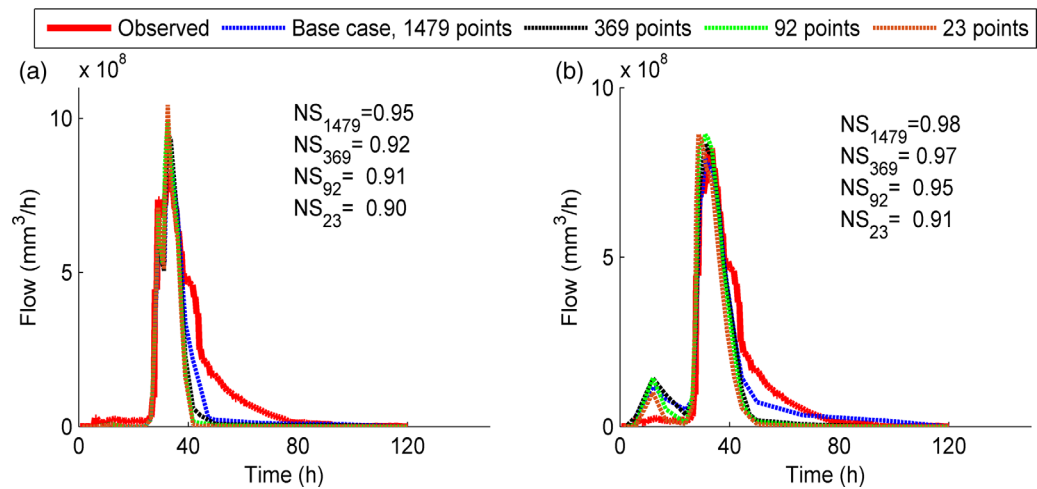


Figure 11. Comparison between subsurface storm flow hydrograph obtained based on different number of soil depth measurements, using (a) OF model and (b) VSSF model. NS represents the Nash Sutcliffe value between simulated (with different resolutions) and observed hydrographs.

based on 369, 92, and 23 measurements. Note that the base case used earlier stems from 1479 measured points along the bedrock and soil surface. All resolutions were then interpolated into a 1 m DEM using kriging to ensure an identical mesh discretization for all simulations. Figure 11 shows the simulated results of the subsurface stormflow hydrograph for the three sets of soil depth measurements using the OF (Figure 11a) and VSSF (Figure 11b) models. The Nash Sutcliffe values for the simulated hydrographs range from 0.90 to 0.97 for all six simulations. Both model results show that a simple realization of soil depth based on only 23 measurements is able to sufficiently mimic the observed stormflow hydrograph similar to realizations generated from 1479 soil depth measurements. Furthermore, simulated results suggest that the VSSF model developed based on only 23 soil depth measurements is able to adequately estimate seepage at the base of the soil ($F(x, y, z, t)$); this seepage is the input term over the bedrock surface in the OF model used to simulate subsurface stormflow. Despite the adequateness of coarse soil depth resolutions in the prediction of overall behavior of response hydrographs, both models are sensitive to soil depth resolutions in the simulation of fine details of the hydrograph. This effect is larger on peak flow value in OF model and hydrograph recession in VSSF model.

In addition, pressure distributions throughout the soil mantle obtained from the VSSF model (for the base case scenario and three cases assessed in this section) show negligible pressure head gradient in x , y , and z directions (with a maximum of 0.10 for all times). This implies that a simple 1-D free drainage model, rather than 3-D variably saturated subsurface model, may provide a reasonable approximation of the seepage flow at the base of the soil mantle ($F(x, y, z, t)$) used in the overland flow model.

4.5. Is the Diffusion Wave Approximation Appropriate?

Here we investigate the effect of local and/or convective inertia, friction, slope, and pressure gradient by obtaining their corresponding terms in the full Saint-Venant equation (equation (2)). Both VSSF and OF models show that the maximum absolute value of the inertia terms in equations (2b) and (2c) (i.e., $\frac{\partial}{\partial t}(d_o \bar{v}_{xo})$, $\frac{\partial}{\partial x}(d_o \bar{v}_{xo}^2)$, $\frac{\partial}{\partial y}(d_o \bar{v}_{xo} \bar{v}_{yo})$, $\frac{\partial}{\partial t}(d_o \bar{v}_{yo})$, $\frac{\partial}{\partial y}(d_o \bar{v}_{yo}^2)$ and $\frac{\partial}{\partial x}(d_o \bar{v}_{xo} \bar{v}_{yo})$) is on the order of 10^{-11} (m^2/s^2); 7–10 orders of magnitude less than the remaining terms in equations (2b) and (2c), i.e., $gd_o \frac{\partial(d_o)}{\partial x}$, $gd_o(S_{ox} - S_{fx})$, $gd_o \frac{\partial(d_o)}{\partial y}$, and $gd_o(S_{oy} - S_{fy})$ which ranged between 10^{-4} and 10^{-1} (m^2/s^2). The assumption is additionally supported by the lack of depressions along the bedrock topography (i.e., no expectation of backwater effect). Both suggest that the negligible inertia assumption is valid and the diffusion wave model used here to simulate subsurface stormflow is equivalent to the full Saint-Venant equation. If we assume (as is typically done) that the Saint-Venant model is the proper choice for simulating shallow overland flow, this implies that the behavior of subsurface stormflow and overland flow are mathematically very similar under the conditions at Panola, which may justify the use of an overland flow approach to represent subsurface stormflow. These calculations also suggest that the pressure gradient terms ($gd_o \frac{\partial(d_o)}{\partial x}$, $gd_o \frac{\partial(d_o)}{\partial y}$) are the

largest terms in equations (2b) and (2c) with a maximum absolute value of 10^{-1} (m^2/s^2). This implies that the effect of spatial variation of subsurface stormflow depth along the bedrock interface is not negligible and a kinematic wave model which typically ignores this effect would not be valid for simulating subsurface stormflow at the Panola slope. Lastly, both VSSF and OF models show that the maximum Froude number values for all test cases were well below 1. This supports the subcritical flow assumption used for the development of the OF model.

5. Discussion

Our results suggest that a diffusion wave overland flow model can mimic the main characteristics of hillslope-scale subsurface stormflow routing along the soil-bedrock interface. This includes the timing of flow initiation, total magnitude of flow, and flow recession. Furthermore, the overland flow model can do so as accurately as a variably saturated, Darcy-Richards subsurface flow model for a range of rainfall depths and slopes as long as measureable subsurface stormflow occurs. Of course, this is only the case as long as the soil "removal" in the overland flow model is "compensated for" by otherwise precisely estimating drainage from the soil to be used as input to the bedrock surface and by using an appropriate Manning coefficient. The alternative overland flow model with a transferred precipitation as input to the bedrock surface (OF_{prec}), instead of using a precise soil seepage, could somewhat approximate the observed hydrograph timing and overall runoff and bedrock infiltration coefficient, but slightly overestimates peak runoff. It is clear that the mediation of the soil mantle is an important control on peak flows.

Both VSSF and OF models are able to capture the spatial and temporal dynamics of the bedrock interface in terms of deep percolation into the bedrock and lateral subsurface stormflow above the interface. These findings are thus notable for two reasons: (1) they support the recent suggestion by *McDonnell* [2013] that subsurface stormflow and overland flow share striking similarities, in terms of the combination and sequence of detention storage, filling and spilling of detention elements, loss to the infiltrating zone below, ultimate connectivity of the saturated patches and then threshold response at the hillslope outlet, and (2) the extreme computational savings of the diffusion wave approach (particularly as rainfall depth and slope increase) and the opportunities it might open up for modeling subsurface stormflow in steep basins with similar behavior as the Panola (e.g., negligible exfiltration from the bedrock groundwater vertically upward into the soil profile).

5.1. Infiltration Excess Subsurface Stormflow

The observed similarity between subsurface stormflow and overland flow raises the following questions: does infiltration excess overland flow occur at depth? Are there any subsurface controls on infiltration at depth that effectively lead to infiltration excess behavior? Figure 12a depicts the time history of simulated bedrock infiltration, soil seepage over the bedrock and runoff at the trench using both the VSSF and OF models. This figure indicates that the bedrock infiltration rate is equal to soil seepage rate into the bedrock (e.g., at time (1)) before the storm begins. At $t = 10$ h, drainage flux from the soil exceeds the infiltration capacity of the underlying bedrock and runoff at the trench begins. Nevertheless, at this time, the trench flow is minimal. During the major precipitation event, the soil seepage rate over the bedrock considerably exceeds the bedrock infiltration capacity (e.g., at time (2)) and at $t = 27.5$ h significant subsurface stormflow at the trench face is activated. This mechanism is depicted schematically in Figure 12b. Initial bedrock abstraction in the figure represents the bedrock infiltration rate before the emergence of patches of saturation along the bedrock. Continuing bedrock abstraction represents the bedrock infiltration rate after flow activation. Figure 12b indicates that at time (1), the rate of soil seepage over the bedrock is less than bedrock infiltration capacity and therefore bedrock infiltration rate (initial abstraction) is equal to the rate of soil seepage over the bedrock without subsurface stormflow. At time (2), the relative rate of soil seepage over the bedrock is larger than the bedrock's infiltration capacity; this excess soil seepage over the bedrock leads to subsurface stormflow activation along the slope while the bedrock infiltration rate (continuing abstraction) is equal to bedrock infiltration capacity. When soil seepage over the bedrock decreases to less than bedrock infiltration capacity, the bedrock infiltration rate again becomes equal to the rate of soil seepage over the bedrock, deactivating subsurface stormflow.

This mechanism is directly analogous to infiltration excess overland flow [e.g., *Green and Ampt*, 1911; *Philip*, 1957] and is effectively infiltration excess subsurface stormflow. The primary difference is that the former is

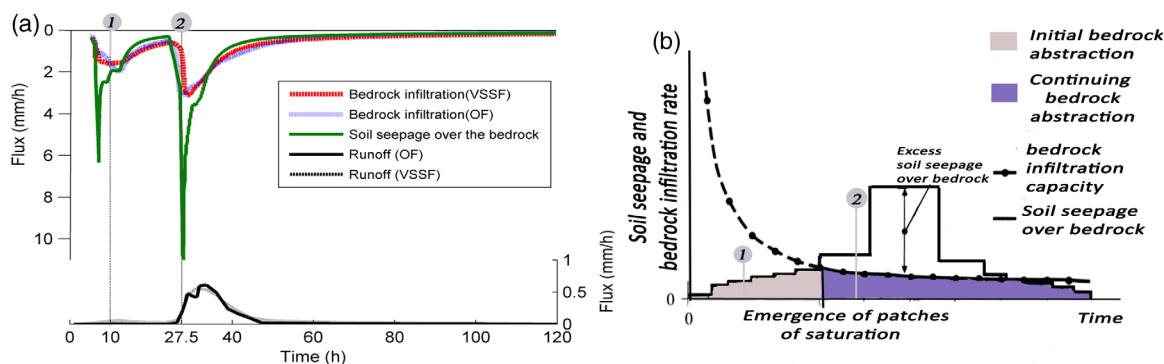


Figure 12. Layout of infiltration excess subsurface storm flow along the bedrock. (a) Top figure shows the simulated soil seepage flux over the bedrock, simulated bedrock infiltration flux using VSSF model and simulated bedrock infiltration flux using OF model. Bottom figure depicts simulated runoff flux at the trench using VSSF and OF models. Grey lines show the activation of subsurface storm flow at $t = 10$ h and $t = 27.5$ h, and times (1) and (2) refer to period before and after major storm flow activation. (b) The conceptual model of infiltration excess subsurface storm flow.

controlled by soil surface infiltration capacity and the latter is controlled by bedrock infiltration capacity. Note that both variably saturated subsurface and overland flow models presented in this paper predict infiltration excess subsurface stormflow in a similar fashion.

5.2. Are All Runoff Forms Diffusive?

Diffusion wave and kinematic wave equations are widely used in the simulation of 1-D and 2-D shallow overland flow [e.g., Almeida and Bates, 2013; Gottardi and Venutelli, 2008; Kazezyilmaz-Alhan and Medina, 2007; Singh, 2001, 2002]. Software packages also employ these equations for simulation of overland flow [Hughes and Liu, 2008; Scharffenberg and Fleming, 2006]. The pressure gradient term (the fourth term in equations (2b) and (2c)), which is ignored in the kinematic wave model, represents the spatial variability of overland flow depth. Overland flow depth is not always uniform, particularly when land surface contains microtopographic structures. Therefore, the implementation of kinematic wave approach may only be valid for flow over a very steep slope [Singh, 2002], where the impact of microtopographic structures is attenuated and ignoring the pressure gradient term is feasible.

Similarities between overland flow and subsurface stormflow behavior may suggest that kinematic wave and diffusion wave models can also be used for the simulation of subsurface stormflow along the soil-bedrock interface. However, the hypothesis that both subsurface stormflow and overland flow are kinematic was generally rejected by Singh [2001, 2002]. Our findings support the idea of Singh [2001, 2002] and suggest that the behavior of subsurface stormflow at the soil-bedrock interface cannot be properly emulated using the kinematic wave approximation. Our results show that the pressure (depth) gradient term has the largest value among all terms in the Saint-Venant equation; this implies that the distribution of subsurface stormflow depth along the bedrock is nonuniform. On the other hand, the diffusion wave equation was found to be efficient in the simulation of subsurface stormflow routing along the Panola slope where pressure (depth) gradient along the bedrock was accurately considered. This combination of findings provides support for the premise that infiltration excess subsurface stormflow is diffusive along the Panola slope and this diffusivity is expressed for a range of slopes and rainfall depths.

5.3. Is There Any Advantage to Using an Overland Flow Model to Simulate Subsurface Stormflow?

Richards' equation [Richards, 1931] (based on Buckingham-Darcy Law) has been widely used to simulate the matrix flow portion of subsurface stormflow at low Reynolds numbers [Ebel et al., 2007b; Lanni et al., 2013; Loague et al., 2010; Mirus and Loague, 2013; Mirus et al., 2007]. These models typically suffered from high-computational cost because of the high grid resolution, very small time steps required and strong nonlinear relationship between material properties and saturation. For instance, Frei et al. [2010] reported a 2 month computational time for performing a simulation of 1 year in duration. Our VSSF model, like all such models, had a long run time. The base case simulations reported here took 3 days using a i7-3370 CPU@3.40 GHz with a 8 GB RAM and the computational time increased drastically for the examples when slope and rainfall depth increased (8 days). However, the OF and OF_{prec} models for the same problem was much more

efficient, with three orders of magnitude shorter run time with fewer calibrated parameters. Additionally, results show that the goodness of fit between OF and VSSF models improved as bedrock slope and rainfall depth increased. Several groups are using physics-based simulators to explore the parameter space controlling subsurface stormflow generation (see, e.g., works by *Ebel et al.* [2009], *James et al.* [2010], *Mirus and Loague* [2013], and *Mirus et al.* [2007]). The computational savings described here may assist in detailed assessment of major subsurface stormflow controls such as bedrock permeability and topography and examination of how connectivity develops and works at hillslope scales. Because such simulations require many combinations and permutations of factors, the run times prohibit traditional approaches. These assessments with our new approach may include uncertainty and sensitivity analyses where many model runs are required. Of course, the use of an overland flow model with the removal of the soil mantle reduces what can be tested in this regard, but its efficiency in representing the temporal and spatial dynamics of hillslope runoff might promote new research questions where this could serve as a tool for rapid assessment.

We could imagine that the overland flow approach could be used as a learning tool for questions of what to measure with limited effort in ungauged basins. For example, *Seibert and Beven* [2009] used a Monte Carlo analysis approach to predict runoff in 11 forested sites as a weighted ensemble mean of 100 simulations with different parameter sets. They concluded that little runoff data are required to sufficiently identify the model parameters in ungauged test period, if the data are chosen intelligently. Using a similar approach, *McIntyre et al.* [2005] computed the runoff for ungauged basins as an ensemble mean of 10,000 simulations each with different parameter sets. Application of Monte Carlo analysis is computationally feasible only with the use of a simpler model as a simulation engine; however these simulators (e.g., Topmodel, HBV) typically simplify the infiltration into the bedrock in subsurface stormflow modeling. The accurate physically based overland flow model proposed in this paper can perhaps be considered as a robust alternative to conceptual hillslope hydrology models for such purposes for the locations where infiltration excess subsurface stormflow is a dominant runoff process.

Lastly, capillary-based Richards' equation models are not able to properly include fast (preferential) flow as might occur along the soil-bedrock interface. This is because Richards' equation is only valid under the laminar flow assumption (Reynolds number < 1). There might be conditions under which the velocity of subsurface lateral flow is large (e.g., 21 m/h in Maimai experimental hillslope in New Zealand as reported by *Graham and McDonnell* [2010]). Consequently, in these instances, the laminar flow assumption is violated. As *Beven and Germann* [2013] suggested, friction-based models (e.g., the diffusion wave model used here) may be able to emulate fast preferential flow along the soil-bedrock interface better than capillary-based models as long as the inertia terms and back water effects are negligible [cf. *Germann and Di Pietro*, 1999]. Furthermore, employing friction-based models to simulate subsurface stormflow along the soil-bedrock interface may provide an easier and more consistent framework to incorporate macropore flow which can be emulated using either friction-based approaches (e.g., Stokes law [*Germann and Di Pietro*, 1999]), kinematic wave models [*Singh*, 2001, 2002] and film flow processes [*Nimmo*, 2012].

5.4. Need for Future Research

Phenomenologically, infiltration excess subsurface stormflow and infiltration excess overland flow are similar. The diffusion wave overland flow model was able to emulate the behavior of the Richards-based variably saturated flow model along a range of slopes and rainfall depths (as long as measureable subsurface flow was initiated). However, we acknowledge that this conclusion is for the Panola test case only; a situation where there is no contribution of groundwater exfiltration from the bedrock below to subsurface stormflow above [cf. *Ebel et al.*, 2007a,b; *Rempe and Dietrich*, 2014]. Furthermore, at the Panola experimental slope there is no evidence of transition from subsurface stormflow to saturation excess overland flow at topographic convergences [cf. *Mirus and Loague*, 2013]. Although there are many steep forested hillslopes with a similar behavior as the Panola (the Maimai site in New Zealand, the HJ Andrews site in Oregon and many others reviewed in *Bachmair and Weiler* [2011]), to conclude all runoff processes are the same, of course, requires much further coupled experimental-modeling study. Many environments and settings may reject this thesis—and that itself will be an interesting analysis and rejectable null hypothesis. Other questions regarding the role of soil, and how the Manning coefficient is able to emulate the subsurface stormflow behavior in the OF model need to be further explored—especially where the soil mantle properties vary with depth. Further research is also needed to

assess the ability of OF model to emulate the VSSF model at the watershed scale and in response to sequences of rainfall events with inclusion of evapotranspiration effects.

Ultimately, surface flow and flow through porous media “along the bedrock” represent fundamentally different physical processes where the latter follows so called “creeping” behavior with typically laminar flow and the former follows open channel flow behavior, potentially with turbulent characteristics. However, both overland and subsurface stormflow share a number of critical similarities which makes them challenging to distinguish: both are guided by the topography of a lower surface, both are controlled by the resistance of the media through which storm water flows, and, as seen here, both are decidedly influenced by the infiltration characteristics of the bottom surface. The numerical experiments performed here demonstrate that, even with an extremely well-characterized and heavily monitored hillslope such as the one at the Panola, it is challenging to state whether the overland flow or variably saturated subsurface flow model outperforms the other. This begs the question of whether there is practical utility in differentiating between the two types of flow phenomenon at the hillslope scale or larger, even if the microscale phenomena are clearly distinct. This indistinguishability has implications for future modeling efforts, and we suggest that it will be worthwhile to lean on the very relevant overland flow paradigm during future investigations of subsurface stormflow.

6. Conclusion

We assessed the ability of an overland flow model to simulate infiltration excess subsurface stormflow in comparison to a 3-D variably saturated subsurface flow model for individual rainfall runoff events at the well-studied Panola hillslope. Both approaches were able to replicate the observed hydrograph characteristics including flow initiation, peak and recession. Both models predicted similar infiltration rates to the bedrock and spatial patterns of lateral flow along the bedrock. Examination of different slopes and rainfall depths through virtual experiments further revealed that both models can represent infiltration excess subsurface stormflow similarly for events generating measurable subsurface stormflow. These similarities between overland flow and variably saturated subsurface flow models, and the observed capacity of the infiltration excess overland flow model to accurately simulate infiltration excess subsurface stormflow may suggest that the two behaviors are indeed similar as are the role of their controlling boundaries (the soil surface and the soil-bedrock interface). We suggest that at the Panola bedrock permeability controls the subsurface stormflow mechanism in a manner analogous to how the soil surface controls the generation of infiltration excess overland flow. Our results suggest that hillslope response is less dependent upon soil depth distribution and more dependent on the underlying bedrock permeability. Our simple realizations of soil depth based on a few soil depth measurements were able to emulate the hillslope hydrograph behavior similar to realizations based on many soil depth measurements. The simulated pressure head gradient throughout the soil mantle also suggested that a simple 1-D free drainage model may efficiently represent the subsurface flow in the soil mantle. Although these conclusions are made strictly for Panola, we believe that they can be extended to other steep forested hillslopes with similar fill and spill runoff behavior.

Our work suggests that application of an overland flow model to subsurface stormflow may be worth further exploration. The variably saturated Darcy-Richards model is highly sensitive to nonlinear unsaturated parameters of the soil. Computationally, the Darcy-Richards solver is three orders of magnitude slower than the overland flow-based model which may nominate the latter model for application to Monte-Carlo, sensitivity and uncertainty analyses where many model runs are required. Finally, recognition of the similarities between overland flow and subsurface stormflow may enable field hydrologists and modelers to develop alternative modeling approaches using models as learning tools and for prediction in ungauged basins.

Acknowledgments

We thank Ali Sarhai, Mahsa Jessri, Willemijn Appels, Ilja van Meerveld, Chris Graham, Jessica Liggett, Tommaso Moramarco, Sven Frei, and Luisa Hopp for useful conversations. We appreciate the feedback of anonymous reviewers and associate editor of Water Resources Research journal. We thank Aquanty, Inc. for the provision of the HydroGeoSphere software used in this experiment. This research was funded by a 2014 NSERC Discovery grant and NSERC Accelerator grant to J. J. M. The data used for all simulations are available upon request from the corresponding author.

References

- Almeida, G. A., and P. Bates (2013), Applicability of the local inertial approximation of the shallow water equations to flood modeling, *Water Resour. Res.*, 49, 4833–4844, doi:10.1002/wrcr.20366.
- Antoine, M., M. Javaux, and C. Bièdiers (2009), What indicators can capture runoff-relevant connectivity properties of the micro-topography at the plot scale?, *Adv. Water Resour.*, 32(8), 1297–1310.
- Appels, W., J. Freer, C. Graham, and J. J. McDonnell (2015), Factors affecting the spatial pattern of bedrock groundwater recharge at the hillslope scale, *Hydrol. Processes*, 29, 4594–4610, doi:10.1002/hyp.10481.
- Bachmair, S., and M. Weiler (2011), New dimensions of hillslope hydrology, in *Forest Hydrology and Biogeochemistry*, edited by D. Levia, D. Carlyle-Moses, and T. Tanaka, pp. 455–481, Springer, Netherlands.

- Beven, K. (1981), Kinematic subsurface stormflow, *Water Resour. Res.*, 17(5), 1419–1424.
- Beven, K. (1982), On subsurface stormflow: Predictions with simple kinematic theory for saturated and unsaturated flows, *Water Resour. Res.*, 18(6), 1627–1633.
- Beven, K. (2006), Searching for the Holy Grail of scientific hydrology, *Hydrol. Earth Syst. Sci. Discuss.*, 10(5), 609–618.
- Beven, K., and P. Germann (2013), Macropores and water flow in soils revisited, *Water Resour. Res.*, 49, 3071–3092, doi:10.1002/wrcr.20156.
- Burns, D. A., R. P. Hooper, J. J. McDonnell, J. E. Freer, C. Kendall, and K. Beven (1998), Base cation concentrations in subsurface flow from a forested hillslope: The role of flushing frequency, *Water Resour. Res.*, 34(12), 3535–3544.
- Chu, X., J. Yang, Y. Chi, and J. Zhang (2013), Dynamic puddle delineation and modeling of puddle-to-puddle filling-spilling-merging-splitting overland flow processes, *Water Resour. Res.*, 49, 3825–3829, doi:10.1002/wrcr.20286.
- Clark, M. P., A. G. Slater, D. E. Rupp, R. A. Woods, J. A. Vrugt, H. V. Gupta, T. Wagener, and L. E. Hay (2008), Framework for Understanding Structural Errors (FUSE): A modular framework to diagnose differences between hydrological models, *Water Resour. Res.*, 44, W00B02, doi:10.1029/2007WR006735.
- Costabile, P., C. Costanzo, and F. Macchione (2012), Comparative analysis of overland flow models using finite volume schemes, *J. Hydroinform.*, 14(1), 122–135.
- Ebel, B. A., K. Loague, W. E. Dietrich, D. R. Montgomery, R. Torres, S. P. Anderson, and T. W. Giambelluca (2007a), Near-surface hydrologic response for a steep, unchanneled catchment near Coos Bay, Oregon. 1: Sprinkling experiments, *Am. J. Sci.*, 307(4), 678–708.
- Ebel, B. A., K. Loague, J. E. Vanderkwaak, W. E. Dietrich, D. R. Montgomery, R. Torres, and S. P. Anderson (2007b), Near-surface hydrologic response for a steep, unchanneled catchment near Coos Bay, Oregon. 2: Physics-based simulations, *Am. J. Sci.*, 307(4), 709–748.
- Ebel, B. A., B. B. Mirus, C. S. Heppner, J. E. Vanderkwaak, and K. Loague (2009), First-order exchange coefficient coupling for simulating surface water-groundwater interactions: Parameter sensitivity and consistency with a physics-based approach, *Hydrol. Processes*, 23(13), 1949–1959.
- Ebel, B. A., K. Loague, and R. I. Borja (2010), The impacts of hysteresis on variably saturated hydrologic response and slope failure, *Environ. Earth Sci.*, 61(6), 1215–1225.
- Fiedler, F. R., and J. A. Ramirez (2000), A numerical method for simulating discontinuous shallow flow over an infiltrating surface, *Int. J. Numer. Methods Fluids*, 32(2), 219–239.
- Freer, J., J. J. McDonnell, K. J. Beven, D. Brammer, D. Burns, R. Hooper, and C. Kendall (1997), Topographic controls on subsurface storm flow at the hillslope scale for two hydrologically distinct small catchments, *Hydrol. Processes*, 11, 1347–1352.
- Freer, J., J. J. McDonnell, K. J. Beven, N. E. Peters, D. A. Burns, R. P. Hooper, B. Aulenbach, and C. Kendall (2002), The role of bedrock topography on subsurface storm flow, *Water Resour. Res.*, 38(12), 1269, doi:10.1029/2001WR000872.
- Frei, S., and J. H. Fleckenstein (2014), Representing effects of micro-topography on runoff generation and sub-surface flow patterns by using superficial rill/depression storage height variations, *Environ. Modell. Software*, 52, 5–18.
- Frei, S., G. Lischeid, and J. H. Fleckenstein (2010), Effects of micro-topography on surface-subsurface exchange and runoff generation in a virtual riparian wetland—A modeling study, *Adv. Water Resour.*, 33(11), 1388–1401.
- Gabrielli, C. P., J. J. McDonnell, and W. T. Jarvis (2012), The role of bedrock groundwater in rainfall-runoff response at hillslope and catchment scales, *J. Hydrol.*, 450–451, 117–133.
- Germann, P. F., and L. Di Pietro (1999), Scales and dimensions of momentum dissipation during preferential flow in soils, *Water Resour. Res.*, 35(5), 1443–1454.
- Gottardi, G., and M. Venutelli (2008), An accurate time integration method for simplified overland flow models, *Adv. Water Resour.*, 31(1), 173–180.
- Graham, C. B., and J. J. McDonnell (2010), Hillslope threshold response to rainfall. (2): Development and use of a macroscale model, *J. Hydrol.*, 393(1–2), 77–93.
- Green, W. H., and G. Ampt (1911), Studies on soil physics. 1: The flow of air and water through soils, *J. Agric. Sci.*, 4(1), 1–24.
- Hopp, L., and J. J. McDonnell (2009), Connectivity at the hillslope scale: Identifying interactions between storm size, bedrock permeability, slope angle and soil depth, *J. Hydrol.*, 376(3–4), 378–391.
- Hopp, L., and J. J. McDonnell (2011), Examining the role of throughfall patterns on subsurface stormflow generation, *J. Hydrol.*, 409(1–2), 460–471.
- Hughes, J. D., and J. Liu (2008), MIKE SHE: Software for integrated surface water/ground water modeling, *Ground Water*, 46(6), 797–802.
- James, A. L., J. J. McDonnell, I. Tromp-van Meerveld, and N. E. Peters (2010), Gypsies in the palace: Experimentalist's view on the use of 3-D physics-based simulation of hillslope hydrological response, *Hydrol. Processes*, 24(26), 3878–3893.
- Jencso, K. G., and B. L. McGlynn (2011), Hierarchical controls on runoff generation: Topographically driven hydrologic connectivity, geology, and vegetation, *Water Resour. Res.*, 47, W11527, doi:10.1029/2011WR010666.
- Kazeyilmaz-Alhan, C. M., and M. A. Medina Jr. (2007), Kinematic and diffusion waves: Analytical and numerical solutions to overland and channel flow, *J. Hydraul. Eng.*, 133(2), 217–228.
- Keim, R., H. Tromp-van Meerveld, and J. McDonnell (2006), A virtual experiment on the effects of evaporation and intensity smoothing by canopy interception on subsurface stormflow generation, *J. Hydrol.*, 327(3), 352–364.
- Lanni, C., J. McDonnell, L. Hopp, and R. Rigon (2013), Simulated effect of soil depth and bedrock topography on near-surface hydrologic response and slope stability, *Earth Surf. Processes Landforms*, 38(2), 146–159.
- Liggett, J. E., A. D. Werner, and C. T. Simmons (2012), Influence of the first-order exchange coefficient on simulation of coupled surface-subsurface flow, *J. Hydrol.*, 414–415, 503–515.
- Loague, K., C. S. Heppner, B. A. Ebel, and J. E. Vanderkwaak (2010), The quixotic search for a comprehensive understanding of hydrologic response at the surface: Horton, Dunne, Dunton, and the role of concept-development simulation, *Hydrol. Processes*, 24(17), 2499–2505.
- Manning, R., J. P. Griffith, T. Pigot, and L. F. Vernon-Harcourt (1890), On the flow of water in open channels and pipes, *Trans. Inst. Civ. Eng. Ireland*, 20(1889), 161–166.
- Massey F. J., Jr. (1951), The Kolmogorov-Smirnov test for goodness of fit, *J. Am. Stat. Assoc.*, 46(253), 68–78.
- McDonnell, J. J. (2013), Are all runoff processes the same?, *Hydrol. Processes*, 27(26), 4103–4111.
- McDonnell, J. J., J. Freer, R. Hooper, C. Kendall, D. Burns, K. Beven, and J. Peters (1996), New method developed for studying flow on hill-slopes, *Eos Trans. AGU*, 77(47), 465–472.
- McDonnell, J. J., et al. (2007), Moving beyond heterogeneity and process complexity: A new vision for watershed hydrology, *Water Resour. Res.*, 43, W07301, doi:10.1029/2006WR00546.
- McIntosh, J., J. J. McDonnell, and N. E. Peters (1999), Tracer and hydrometric study of preferential flow in large undisturbed soil cores from the Georgia Piedmont, USA, *Hydrol. Processes*, 13(2), 139–155.

- McIntyre, N., H. Lee, H. Wheeler, A. Young, and T. Wagener (2005), Ensemble predictions of runoff in ungauged catchments, *Water Resour. Res.*, *41*, W12434, doi:10.1029/2005WR004289.
- McLaren, R. (2004), *GRID BUILDER, a Pre-Processor for 2-D, Triangular Element, Finite-Element Programs*, Groundwater Simul. Group, Univ. of Waterloo, Waterloo, Ont., Canada.
- Mirus, B. B. (2015), Evaluating the importance of characterizing soil structure and horizons in parameterizing a hydrologic process model, *Hydrol. Processes*, *29*(21), 4611–4623.
- Mirus, B. B., and K. Loague (2013), How runoff begins (and ends): Characterizing hydrologic response at the catchment scale, *Water Resour. Res.*, *49*, 2987–3006, doi:10.1002/wrcr.20218.
- Mirus, B. B., B. A. Ebel, K. Loague, and B. C. Wemple (2007), Simulated effect of a forest road on near-surface hydrologic response: Redux, *Earth Surf. Processes Landforms*, *32*(1), 126–142.
- Modarres, R. (2010), Regional dry spells frequency analysis by L-moment and multivariate analysis, *Water Resour. Manage.*, *24*(10), 2365–2380.
- Nash, J. (1959), Systematic determination of unit hydrograph parameters, *J. Geophys. Res.*, *64*(1), 111–115.
- Nash, J., and J. V. Sutcliffe (1970), River flow forecasting through conceptual models. Part I—A discussion of principles, *J. Hydrol.*, *10*(3), 282–290.
- Nimmo, J. R. (2012), Preferential flow occurs in unsaturated conditions, *Hydrol. Processes*, *26*(5), 786–789.
- Olkin, I. (1960), *Contributions to Probability and Statistics: Essays in Honor of Harold Hotelling*, Stanford Univ. Press, Stanford, Calif.
- Peters, N. E., J. Freer, and B. T. Aulenbach (2003), Hydrological dynamics of the Panola Mountain Research Watershed, Georgia, *Ground Water*, *41*(7), 973–988.
- Philip, J. R. (1957), The theory of infiltration. 4: Sorptivity and algebraic infiltration equations, *Soil Sci.*, *84*(3), 257–264.
- Rempe, D. M., and W. E. Dietrich (2014), A bottom-up control on fresh-bedrock topography under landscapes, *Proc. Natl. Acad. Sci. U. S. A.*, *111*(18), 6576–6581.
- Richards, L. A. (1931), Capillary conduction of liquids through porous mediums, *Physics N. Y.*, *1*(5), 318–333.
- Scharffenberg, W. A., and M. J. Fleming (2006), *Hydrologic Modeling System HEC-HMS: User's Manual*, U.S. Army Corps of Eng., Hydrol. Eng. Cent, Davis, Calif.
- Seibert, J., and K. J. Beven (2009), Gauging the ungauged basin: How many discharge measurements are needed?, *Hydrol. Earth Syst. Sci.*, *13*(6), 883–892.
- Singh, V. (2001), Kinematic wave modelling in water resources: A historical perspective, *Hydrol. Processes*, *15*(4), 671–706.
- Singh, V. (2002), Is hydrology kinematic?, *Hydrol. Processes*, *16*(3), 667–716.
- Sloan, P. G., and I. D. Moore (1984), Modeling subsurface stormflow on steeply sloping forested watersheds, *Water Resour. Res.*, *20*(12), 1815–1822.
- Spence, C., and M.-K. Woo (2003), Hydrology of subarctic Canadian shield: Soil-filled valleys, *J. Hydrol.*, *279*(1), 151–166.
- Therrien, R., R. McLaren, E. Sudicky, and S. Panday (2008), *HydroGeoSphere: A Three-Dimensional Numerical Model Describing Fully-Integrated Subsurface and Surface Flow and Solute Transport*, Groundwater Simul. Group, Waterloo, Ont., Canada.
- Tromp-van Meerveld, H. J., and J. J. McDonnell (2006a), Threshold relations in subsurface stormflow. 1: A 147-storm analysis of the Panola hillslope, *Water Resour. Res.*, *42*, W02410, doi:10.1029/2004WR003778.
- Tromp-van Meerveld, H. J., and J. J. McDonnell (2006b), Threshold relations in subsurface stormflow. 2: The fill and spill hypothesis, *Water Resour. Res.*, *42*, W02411, doi:10.1029/2004WR003800.
- Tromp-van Meerveld, H. J., N. E. Peters, and J. J. McDonnell (2007), Effect of bedrock permeability on subsurface stormflow and the water balance of a trenched hillslope at the Panola Mountain Research Watershed, Georgia, USA, *Hydrol. Processes*, *21*(6), 750–769.
- Tromp-van Meerveld, H. J., A. L. James, J. J. McDonnell, and N. E. Peters (2008), A reference data set of hillslope rainfall-runoff response, Panola Mountain Research Watershed, United States, *Water Resour. Res.*, *44*, W06502, doi:10.1029/2007WR006299.
- Weiler, M., and J. McDonnell (2004), Virtual experiments: A new approach for improving process conceptualization in hillslope hydrology, *J. Hydrol.*, *285*(1–4), 3–18.
- White, A., A. E. Blum, M. S. Schulz, T. G. Huntington, N. E. Peters, and D. A. Stonestrom (2002), Chemical weathering of the Panola Granite: Solute and regolith elemental fluxes and the weathering rate of biotite, in *Water Rock Interactions, Ore Deposits, and Environmental Geochemistry: A Tribute to David A. Crerar*, edited by R. Hellmann, and S. A. Wood, pp. 37–59, Geochemical Society, Special Publication NO. 7, Davos, Switzerland.